PNL--7589

DE91 007425

FINAL REPORT ON THE CHARACTERIZATION OF THE FILM ON INERT ANODES

C. F. Windisch Jr.
N. D. Stice

January 1991

Prepared for
the U.S. Department of Energy
under Contract DE-AC06-76RLO 1830

Pacific Northwest Laboratory
Richland, Washington 99352

SUMMARY

Results of post-test microscopic and elemental analysis of the reaction zone on polarized cermet inert anodes, over a range of current densities and alumina concentrations, suggest that an alumina film does not form to protect the anode from dissolution. Rather, significant morphological and compositional changes occur at or near the anode surface. These changes and the chemical reactions that cause them involve the cermet material itself and appear to be responsible for properties that were previously assigned to an alumina film. In particular, a reaction layer formed from the cermet material may have protective properties, while changes in roughness and porosity may contribute to the electrochemical impedance.

ACKNOWLEDGMENTS

The authors acknowledge the assistance of the staff at the Pacific Northwest Laboratory (PNL), in particular the managerial guidance provided by L. G. Morgan, the technical contributions of D. M. Strachan, the microscopy work done by N. T. Saenz and J. M. McCarthy, and the secretarial support by D. L. Schneider. We are also grateful for the programmatic assistance provided by M. J. McMonigle, Office of Conservation and Renewable Energy (CE), U. S. Department of Energy (DOE), Washington, DC, and the Richland Operations Office, DOE.

CONTENTS

FIGURES

TABLES

1.0 INTRODUCTION

Experimental studies conducted at the Pacific Northwest Laboratory (PNL)[(a)] in FY 1988 and early FY 1989 indicated that the cermet inert anodes evaluated by PNL exhibited a characteristic impedance during the electrolytic production of aluminum in bench-scale Hall-Heroult cells. This impedance was found to have the following characteristics (Strachan et al. 1988):

- It was largely resistive in nature.
- It varied as a function of current density, giving a minimum at about 0.5 A/cm^2.
- It appeared to depend on alumina concentration in the electrolyte. In general, the impedance seemed to increase with increasing alumina concentration.
- It exhibited a time dependence. Different anodes gave different impedances at different times after polarization.
- At high current densities (> 1 A/cm^2), discontinuous changes in the impedance occurred, causing "spikes" in the current or voltage data.

Based on these characteristics, PNL originally proposed (Strachan et al. 1988) that a resistive film formed on inert anodes during electrolysis. It was argued that the formation of this film was necessary to protect the inert anode from corrosion reactions that would otherwise occur in the molten electrolyte. It was also proposed that an anode current density of 0.5 A/cm^2 formed a film with optimum passivating-like characteristics. At lower current densities, the film was proposed to be incompletely formed, resulting in corrosion of the cermet's metallic phase. At higher current densities, it was proposed that the film would become too thick and its resistance would become too high to sustain the current density. Consequently, the film would rupture, resulting in sudden and severe corrosion of the electrode's metal phase. The rupturing events in the film were indicated by sudden drops in

---

(a) PNL is operated for the U.S. Department of Energy by Battelle Memorial Institute under Contract DE-AC06-76RLO 1830.

impedance and appeared as "spikes" in the voltage data for a cell under galvanostatic (constant current) control.

It was also proposed (Strachan et al. 1988) that the quality of the film depended on the alumina concentration in the electrolyte. Higher alumina concentrations seemed to favor a more resistive, presumably thicker, film. Consequently, film rupturing behavior was considered to be more likely at high alumina concentration (close to saturation) when current densities were above 0.5 A/cm^2. Problems with reproducibility of the experimental results were encountered, however, when attempts were made to relate anode impedance explicitly to alumina concentration. It was then concluded that the film impedance was dynamic, changing with time and with small fluctuations in cell conditions.

Attempts to identify the composition of the film in FY 1988 were largely unsuccessful (Strachan et al. 1988). Post-mortem X-ray diffraction of frozen electrolyte near the surface region showed the presence of alumina, but it was uncertain whether the alumina was part of a film or simply precipitate that formed on the anode during cool-down.

During FY 1989 and FY 1990, experiments were performed to identify the properties and composition of the film using a variety of techniques. The milestone report titled "Characterization of the Reaction Layer or Film on PNL Inert Anodes: Progress Report for April-December 1989" (Windisch and Stice 1990) discussed the results of electrochemical impedance and potential-step studies. These results suggested that morphological characteristics of the cermet anode, specifically roughness and surface porosity, play an important role in reactions at the anode surface and in determining electrode impedance. These conclusions are supported by microscopic and compositional analyses of the reaction zone. The results of these analyses are reported in this document.

2.0 EXPERIMENTAL PROCEDURES

Experiments were performed using the bench-scale experimental setup shown in Figure 2.1. The electrochemical cell used a three-electrode arrangement. The cermet inert anode was fabricated at PNL (from $NiO/NiFe_2O_4$ oxide and Cu powders) to contain 17% Cu metal by weight according to procedures discussed in previous reports (Strachan et al. 1988). The anode was formed into the shape of a small cylinder with a cross-section of about 1 cm^2. A boron nitride (BN) sheath was used to protect the walls of the anode, allowing only one of its circular faces to be exposed to the electrolyte. This face was finish-sanded with 600-grit SiC paper to ensure that the anode surface in contact with the electrolyte had a similar morphology for all of the anodes used in these studies. The connector bar was a Ni rod that had been brazed to the anode during the fabrication procedure as discussed in previous reports (Strachan et al. 1988). The cathode, or counter electrode, was a graphite crucible that also served as the cell container. The crucible was large enough to hold about 1 kg of electrolyte. No aluminum metal seed was used in

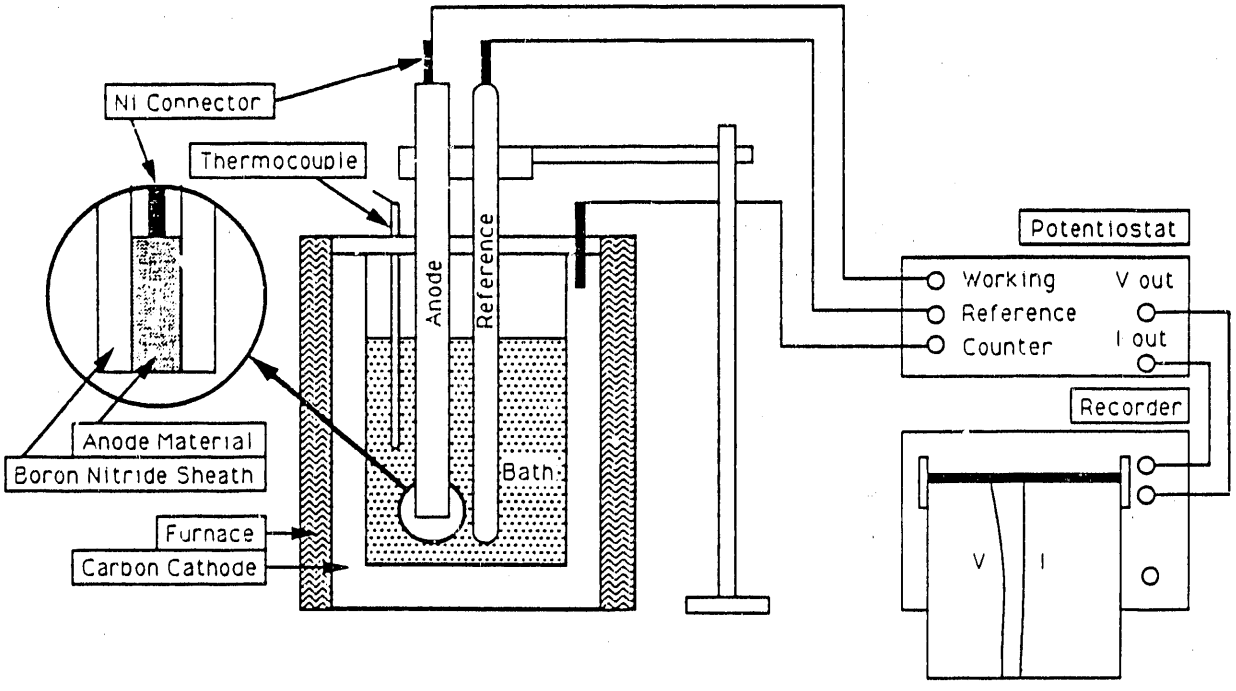

FIGURE 2.1. Apparatus for PNL Bench-Scale Laboratory Tests

these tests. The reference electrode was the Al/Al_2O_3 type, fabricated according to a recently published design (Burgman, Leistra, and Sides 1986).

The electrolyte was prepared by mixing appropriate amounts of reagent grade materials to give a bath ratio (NaF/AlF_3 in wt%) equal to 1.15, 5.5% (by weight) CaF_2, 1.0% MgF_2, and alumina at the desired concentration. Studies were performed with alumina concentrations of 50%, 75%, and 100% of saturation. (Alumina concentrations in this report are given as a percent of saturation, which for these test conditions is approximately 8.0% by weight.) A temperature controller/furnace/thermocouple arrangement was used to melt the raw materials to form a "bath" and control its temperature at 983 ± 2°C. The bath ratio was considered constant and equal to the formulation value (1.15) throughout these short-term tests. As shown in Figure 2.2, the actual variation of bath ratio was negligible within the uncertainties of analysis over the 6-h working life of a laboratory cell.

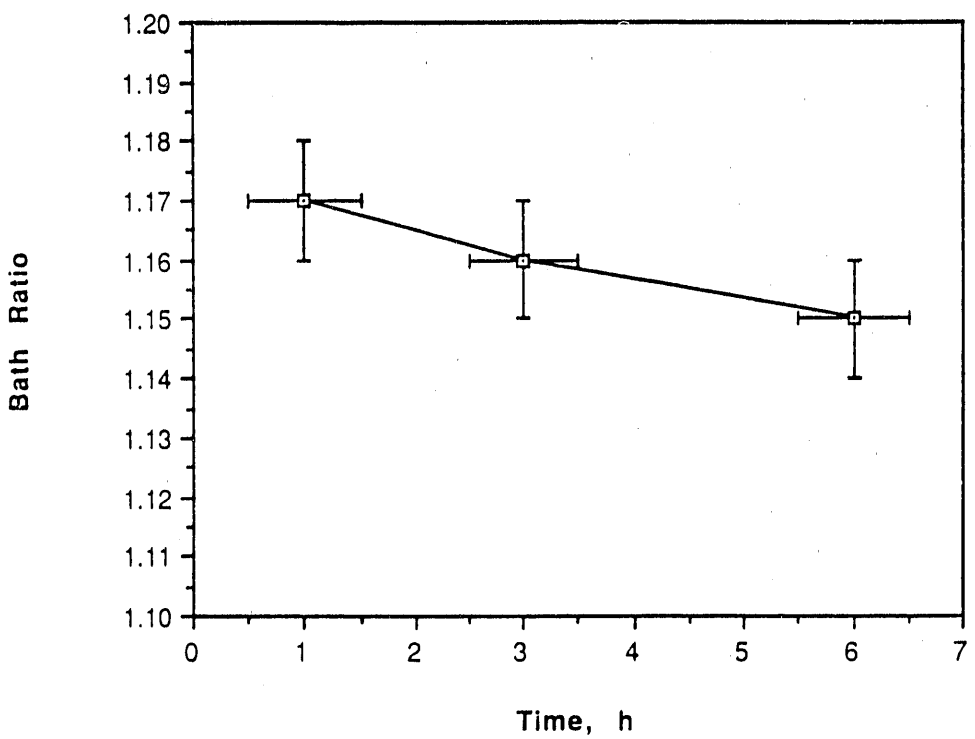

FIGURE 2.2. Variation of Bath Ratio During a Laboratory Test

The anode potential was measured and controlled using a Solartron[a] 1286 Electrochemical Interface. Voltage and current outputs were monitored using a strip chart recorder. A fresh anode was used in each study at a given potential and bath composition. Thus, the results of each test were not subject to variations resulting from previous polarization conditions. Consequently, in a given test, the results could be considered characteristic of only one anode potential and one bath composition.

In a typical test, the bath was first made uniformly molten at 983°C. To remove oxidizable bath impurities, a "preliminary inert anode" was then inserted and polarized to give a current of about 0.5 A for about 1 h. This electrode was then removed and the test anode was inserted. The bath temperature was allowed to reequilibrate, then the potential was set to the desired value while monitoring anode potential and current with a strip chart recorder. The anode was subsequently maintained at the set potential for about 1 h. During this time potential-step data and electrochemical impedance data were collected. (The electrochemical data were discussed in a separate report [Windisch and Stice 1990].) After the 1-h period, the anode was removed from the bath while still under polarization conditions; the voltage was then turned off. The anode was allowed to cool in air and then submitted for analysis using one or more of the following techniques: optical microscopy, scanning electron microscopy (SEM) with energy dispersive X-ray analysis (EDS), electron microprobe, transmission electron microscopy (TEM), and electron diffraction. The entire procedure was then repeated with a new anode at another potential. Bath compositions were changed by starting the test over and using a different compositional mix of raw materials.

For tests with alumina concentrations less than saturation, the reference electrode suffered deterioration because its alumina outer sheath dissolved. As a result, the reference electrode had to be replaced periodically during these studies. Based on approximate weight loss measurements, it was estimated that a maximum end-of-test error of about 10% of saturation was

---

(a) Solartron is a trade name of Solartron Instruments, Farmborough, Hampshire, England.

introduced when the alumina was initially at 50% of saturation (and the dissolution rate of the reference electrode's alumina sheath was a maximum).

3.0 RESULTS AND DISCUSSION

This section covers the results of post-test or *ex situ* studies on the morphology and composition of the reaction layer on cermet inert anodes tested in laboratory cells under various conditions. The bulk[(a)] microstructure and composition of the anodes are first discussed, followed by a description of the original, "pretested," surface morphology and composition. Subsequently, the results of the post-test microscopic and compositional analyses are discussed with emphasis on the effects of anode current density and alumina concentration. Finally, a proposal is made regarding reactions at the anode that explains the results of the analyses and provides some new insight on the effects of microstructure on anode reactions. Recommendations are also made concerning how to optimize anode durability based on the reactions proposed here.

3.1 BULK MORPHOLOGY AND COMPOSITION

The NiO-$NiFe_2O_4$-Cu cermet anodes used in this work had the bulk microstructure shown by the optical micrograph in Figure 3.1. This microstructure had three phases: (a) a nickel-rich oxide phase, (b) a nickel/iron oxide phase, and (c) a metallic phase. Analyses of the three phases for two anodes studied in this work are given in Table 3.1. The results are similar to those reported previously by PNL. The Ni-rich oxide phase, herein referred to as NiO, appears dark grey in the optical micrographs and light grey in the SEM micrographs; the nickel/iron oxide phase, herein referred to as $NiFe_2O_4$ or spinel or ferrite, appears light grey in the optical micrographs and dark grey in the SEM micrographs; the metallic phase, herein referred to as Cu, is the "white" phase in both the optical and SEM micrographs. Black regions are pores or voids in both the optical and SEM micrographs.

(a) The term "bulk," when applied to the anode, refers to subsurface material.

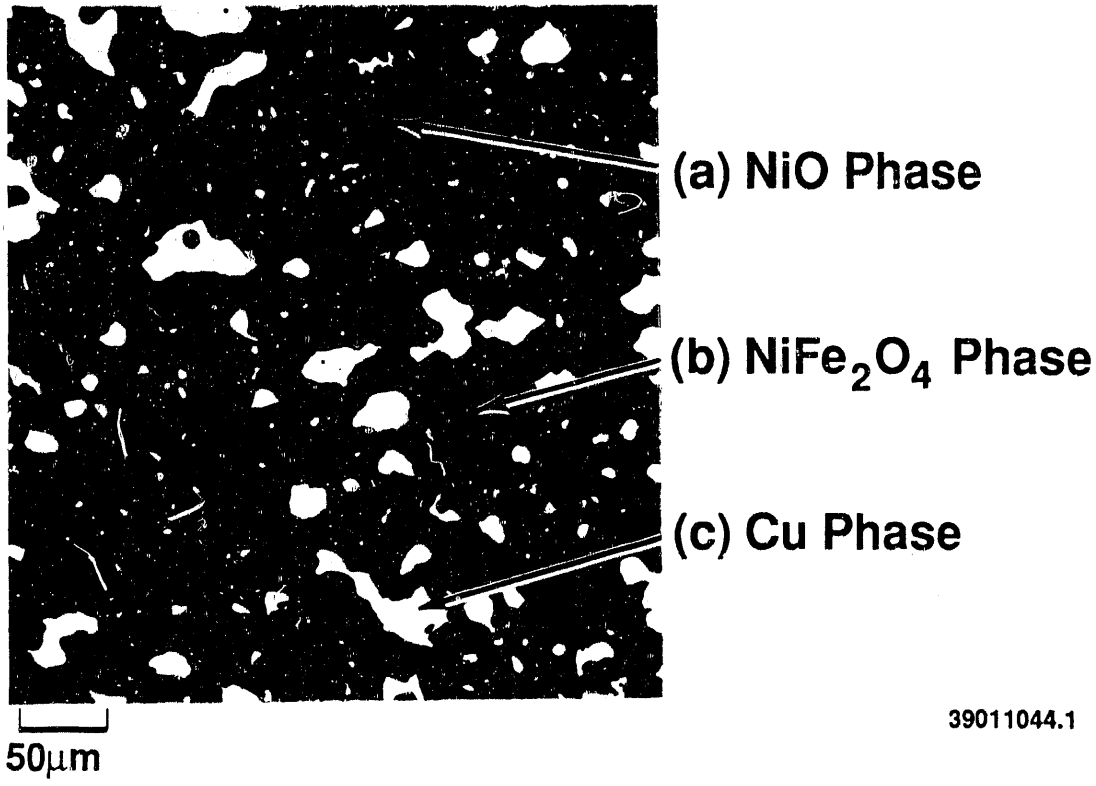

FIGURE 3.1. Bulk Microstructure of Cermet Inert Anode

TABLE 3.1. Elemental Analysis of Bulk Cermet in Weight Percent

Anode	Phase	Na	Al	Si	Ca	Fe	Ni	Cu	Fe/Ni
EAT2SC	NiO	0	0	0.6	0	5.3	60	3.7	0.09
	$NiFe_2O_4$	0	0	0.8	0	43	20	1.1	2.2
EAT3SB	NiO	0	0	0.9	0	10	61	0	0.2
	$NiFe_2O_4$	0	0	0.6	0	47	18	0.9	2.6
	Cu	0	0	0	0	3.2	10	83	0.3
Stoich.	NiO								0
	$NiFe_2O_4$								1.9

It is important to note that the oxide phases, despite being referred to as NiO and $NiFe_2O_4$, were not stoichiometric in composition. This is illustrated in Table 3.1 where the stoichiometric weight ratios of the two oxides are also given. The NiO contained small, but significant, amounts of Fe; the Cu metal phase was actually a Cu-Ni-Fe alloy with Ni as the principal alloying agent. In addition, the spinel phase contained excess Fe. To maintain charge balance, it is reasonable to assume that the excess Fe in the spinel was in the form of Fe^{2+}. (In pure $NiFe_2O_4$, all of the iron is in the form of Fe^{3+}.) The Fe^{2+} probably replaced some of the Ni^{2+} in the oxide lattice.

The average size of the Cu, NiO, and $NiFe_2O_4$ "grains" in the cermet matrix was about 20-50 μm, depending on the sample, the location of analysis, and the phase under study. Distribution of the three phases was considered good, with all phases, in general, uniformly dispersed within the cermet matrix. For the anodes studied in this work, there appeared to be a tendency for the NiO phase to "surround" the Cu metal phase, although this was not always the case. PNL has observed this phenomenon in other NiO-$NiFe_2O_4$-Cu anodes prepared previously. Another interesting structural detail is that, in some cases, a scattering of small, < 1-μm, islands of the $NiFe_2O_4$ phase occurred *within* the larger regions of the NiO phase. Also, some inherent porosity was present in the anodes, although in most cases it was difficult to quantify the porosity using the micrographs alone because of the likelihood that some "pull-out" occurred during the sample mounting procedure.

3.2 SURFACE MORPHOLOGY AND COMPOSITION BEFORE POLARIZATION

The morphology and composition of the surface of the cermet anodes are influenced by the fabrication procedures: in pressing and particularly in sintering. For example, both oxidation of the Cu phase and reduction of the oxide phases during sintering have been observed, depending on the redox state of the furnace atmosphere. Although significant progress has been made in our ability to control the composition of the furnace atmosphere to minimize surface alteration, some effects are still routinely observed. To obtain a reproducible surface morphology for testing in these studies, the to-be-tested

surfaces of all of the anodes in this work were refinished. A thickness of 1 mm or less was removed from the surface of each anode by grinding, followed by a final refinishing step using 600-grit paper.

After refinishing and just prior to using the anodes in the electrolysis tests, the anodes were preheated for a few minutes over the furnace in which the tests were conducted. The preheat was performed to minimize thermal shock. The effects of this preheat step on the surface structure were determined. Figure 3.2 shows the surface of a finished anode that had been preheated and then inserted momentarily in the molten cryolite bath; no electrolysis was performed. The morphology of this anode was considered

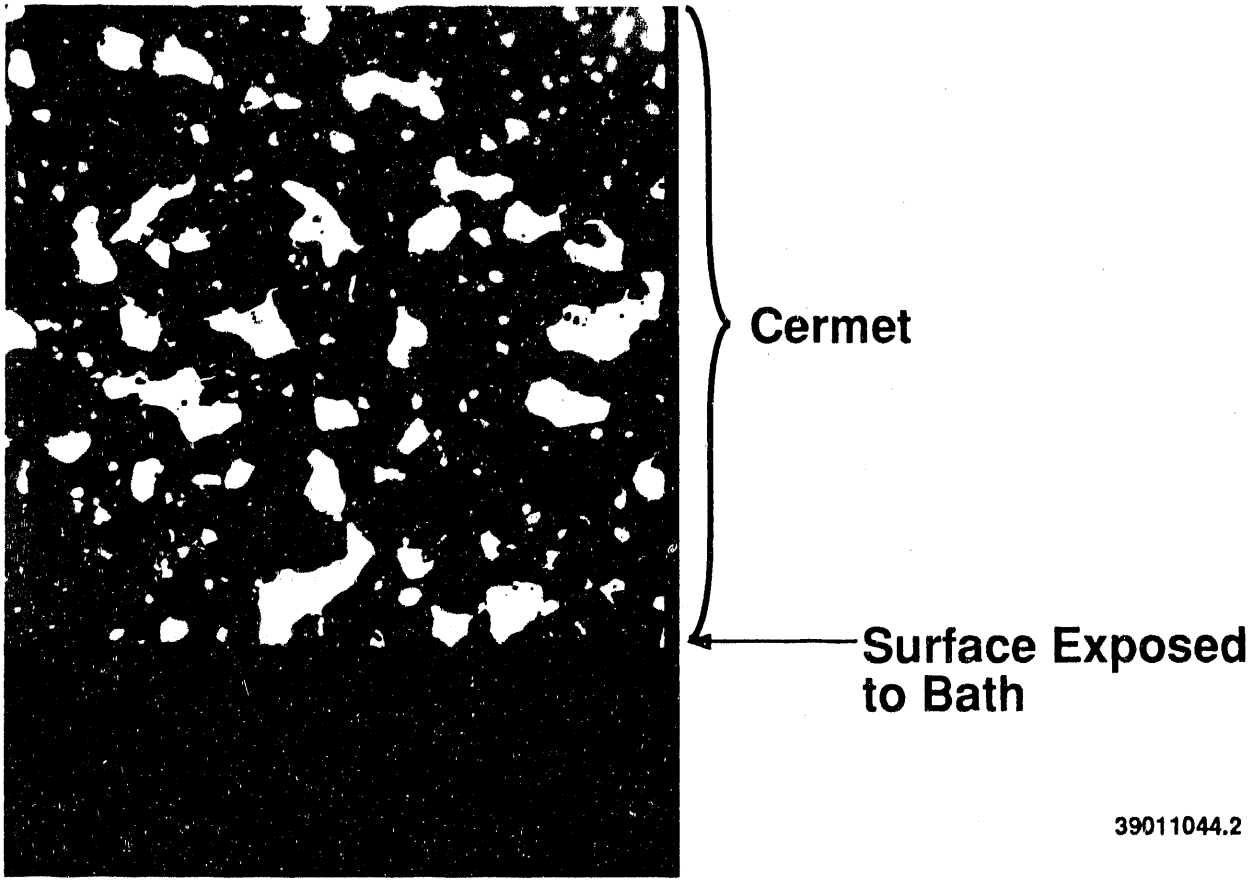

FIGURE 3.2. Optical Micrograph of Surface Region of Cermet Exposed to Molten Bath but Not Polarized

characteristic of all of the anodes used in this work under conditions and at a time *just prior to electrochemical polarization.* Consequently, it served as a baseline surface structure for all of the studies reported here. Any changes in surface structure observed on anodes after polarization were interpreted to reflect the effects of polarization under the conditions studied.

Figure 3.2 shows that, at a magnification of 250X, the surface was reasonably flat with all three phases present at the surface. It is particularly important to note that the metallic Cu phase was also present right at the surface. At a magnification of 1000X, some small amount of surface irregularities were observed. In particular, the oxide phases appeared to be slightly reacted. The extent of reaction was very small, however, with a reaction layer thickness of about 3 μm. This thickness was considered insignificant compared with the irregularities introduced during polarization, which in some cases were approximately an order of magnitude larger.

3.3 SURFACE MORPHOLOGY AFTER POLARIZATION

The effects of anode current density and alumina concentration on the performance of the NiO-$NiFe_2O_4$-Cu cermet anode were evaluated using potential-step methods, electrochemical impedance measurements, and post-test microscopy and compositional analysis of polarized anodes. The results of the potential-step tests and the electrochemical impedance analyses were reported earlier (Windisch and Slice 1990). The complete results of the post-test microscopy studies are discussed in this report. Results of morphological analysis are reported in this section; results of compositional analysis are reported in Section 3.4. Table 3.2 lists the current densities and alumina concentrations for the various anodes that were analyzed using microscopic methods.

Other microscopy data were also obtained on anodes tested in cryolite baths containing added quantities of silica. This work was done to satisfy a previous FY 1990 milestone. Since no significant effect of silica could be ascertained, some of the data from this work are used in subsequent discussions as well.

TABLE 3.2. Test Conditions for Anodes Subjected to Post-Test Microscopy

Sample	Volts[(a)]	Current Density (A/cm^2)	Alumina Saturation (%)
EAT4SA	2.1	0.07	75
EAT4SB	2.4	0.265	75
EAT4SC2	2.5	0.55	75
EAT4SC	2.7	1.0	75
EAT2SB	2.3	0.13	100
EAT3SB	2.4	0.44	100
EAT2SD	2.6	0.8	100
EAT2SC	3.0	1.8	100

(a) Volts versus the Al/Al_2O_3 reference electrode. Bath resistance was estimated to be 0.3 ohm cm^2, giving an anode over voltage of about 0.1 V in these studies.

Figures 3.3(a) through 3.3(d) show the surface region of the anodes polarized in molten cryolite with 75% alumina at various current densities. Figures 3.4(a) through 3.4(d) show the surface region for anodes tested at 100% alumina saturation. Careful examination of the surface microstructures of these anodes suggests a number of important characteristics and trends in morphology as a function of cell operating conditions.

3.3.1 Film Formation

No intact *continuous* film or layer was observed on any of the anodes studied. Compositional data (discussed in Section 3.4) reveal that all of the surface reaction products that could not be simply associated with the frozen cryolitic bath contained significant amounts of the anode components (i.e., Ni, Fe and Cu). This does not support the proposal that a film of alumina forms on cermet inert anodes during polarization and that this film protects them under certain operating conditions. If a film does form, then it appears to be more of a "reaction layer" containing not only bath components but corrosion/dissolution products of the anode as well. Characteristics that have been previously ascribed by PNL to an alumina film, such as

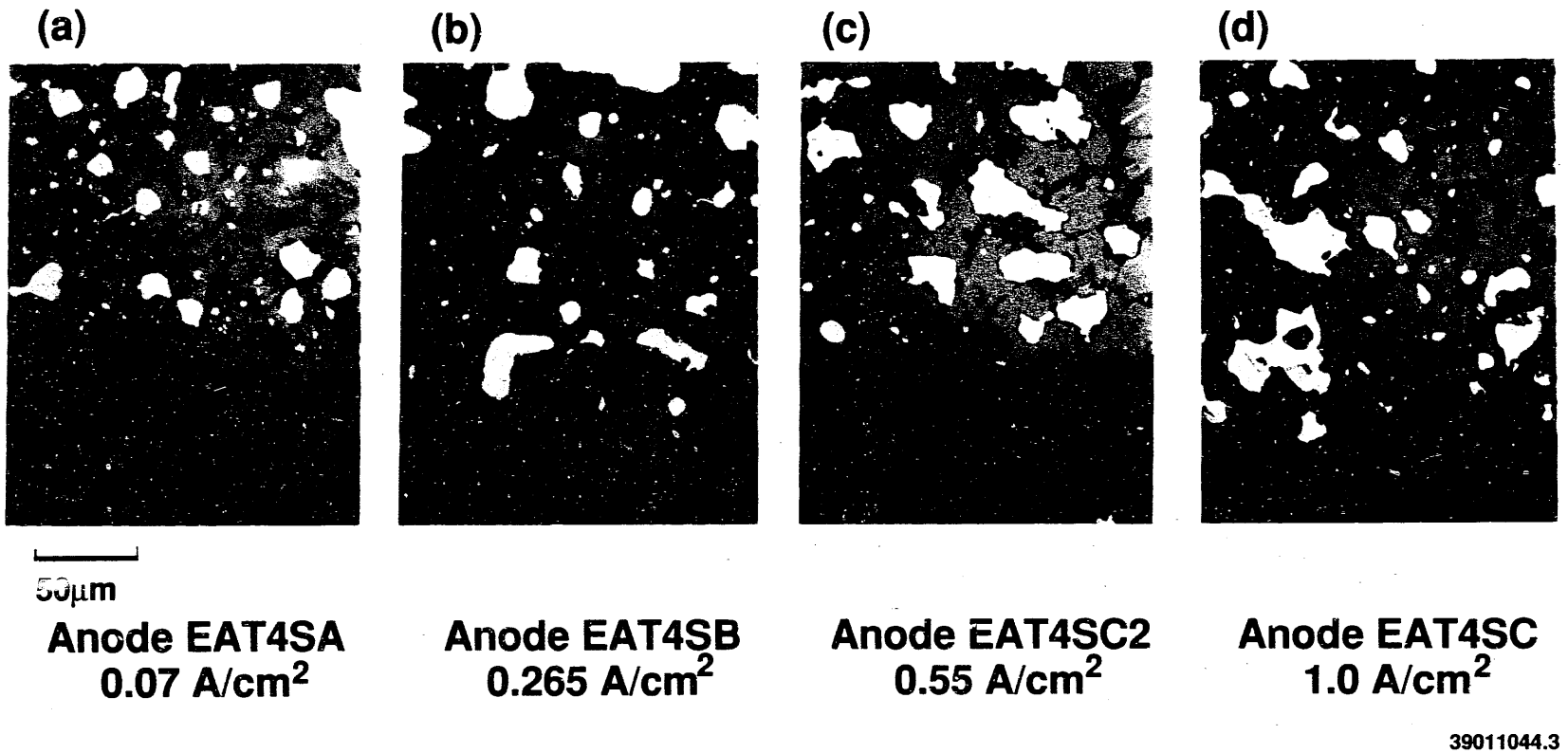

FIGURE 3.3. Optical Micrographs of Surface Region of Cermet Anodes Polarized in Molten Bath Containing 75% Alumina

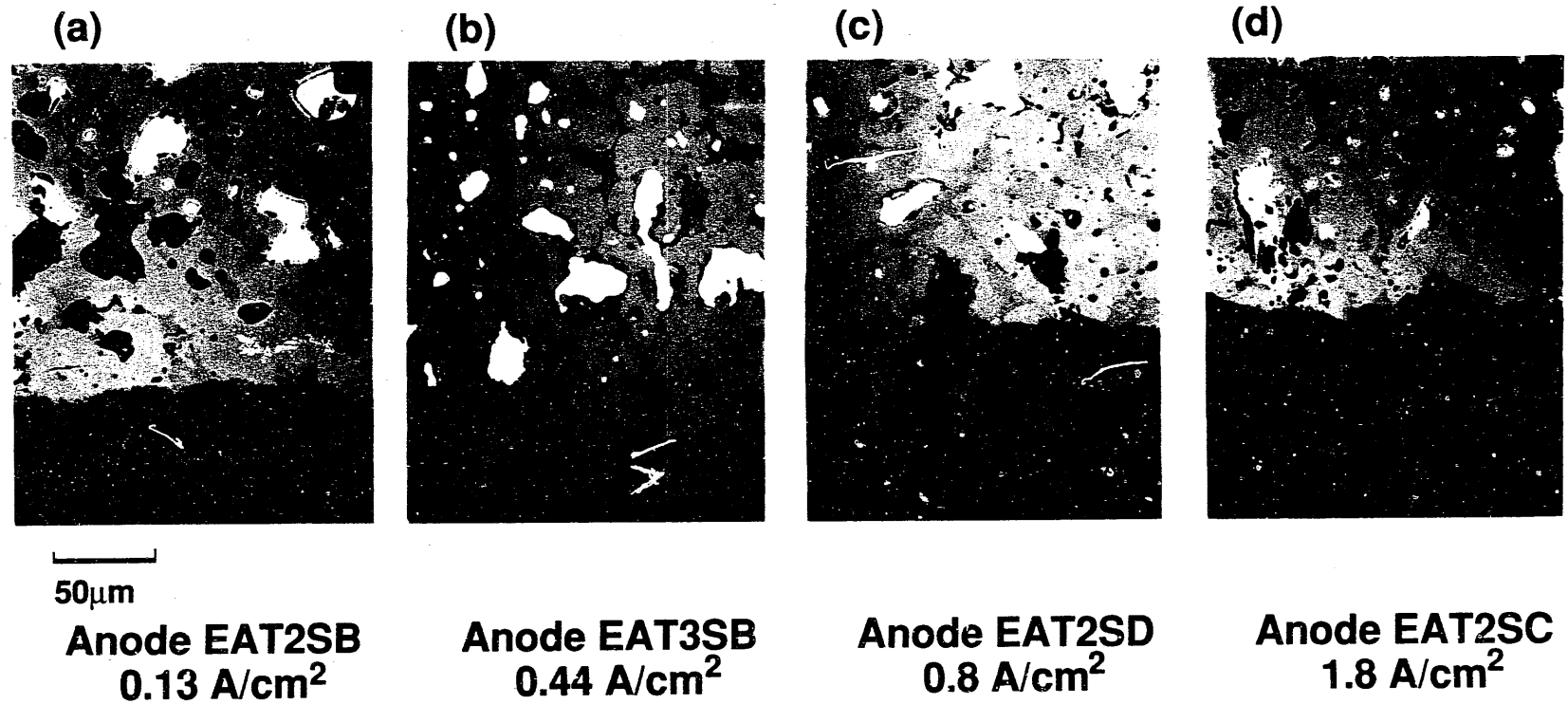

FIGURE 3.4. Optical Micrographs of Surface Region of Cermet Anodes Polarized in Molten Bath Containing 100% Alumina

electrochemical impedance and current/potential spiking, would therefore appear to come from different sources: from the reaction layer, from geometric factors as discussed in Section 3.3.4, or from gas bubbles that behave uniquely on a rough or porous surface.

3.3.2 Low-Current Density Effects

Polarization below 2.2 V, the decomposition potential for alumina in molten cryolite, appears to cause particularly severe corrosion of the cermet anode. As shown in Figure 3.3(a), an anode polarized at 2.1 V and 0.07 A/cm^2 developed significant porosity within a 100-μm distance from the surface. Loss of the Cu metal phase and the development of a dark reaction product also occurred. As shown in Figure 3.4(a), some increase in porosity (although the corrosion was not as severe) was also observed at 2.3 V and 0.13 A/cm^2 at a different alumina concentration.

The mechanism for the corrosion of the cermet anode at low current densities is not certain, but, based on the results of potential-step studies, it appears to be diffusion-controlled and to occur in the cermet's pores. The production of oxygen gas at 2.2 V and above may attenuate this corrosion process by blocking pores in the surface region and reducing access by the molten electrolyte to the Cu metal phase (Windisch and Stice 1990). Another possibility is that the redox conditions present at low oxygen fugacities favor the corrosion/dissolution of the cermet anode. Experiments to resolve this question are planned for FY 1991.

3.3.3 High Current Density Effects

The morphological characteristic that appears most clearly to change as a function of current density is surface roughness. As shown in Figures 3.3 and 3.4, this is particularly the case at current densities above 0.5 A/cm^2 where, at a magnification of 500X, the roughness seems to be the *only* characteristic to vary significantly. The "roughening" may be caused by a difference in reactivity between the three phases. Proposed reactions which support this are presented in Section 3.5, in conjunction with the results of the compositional analysis. In the remainder of Section 3.3, the observed

relationships between surface roughn ss and current density, electrochemical impedance, and alumina concentration, are discussed.

3.3.4 Surface Roughness and Current Density

Examination of Figures 3.3(a) through 3.3(d) reveals that a certain surface roughening appears to accompany polarization of the anode at higher current densities. The roughness was measured for anodes polarized for identical times using exactly the same conditions except for potential, current density, and alumina concentration. Surface roughness was quantified by computing the mean and the standard deviation of numerous measurements of the distance between the anode's surface and a reference point using optical micrographs of the anode sample. The approach is shown schematically in Figure 3.5. The mean, x, gives an indication of the "depth" of the roughness, and the standard deviation, s, measures the extent of "bumpiness." As shown in Figure 3.6, the surface roughness, quantified by parameters x and s, generally decreased as current density increased to about 0.5 A/cm^2. Above 0.5 A/cm^2, the roughness factors increased dramatically.

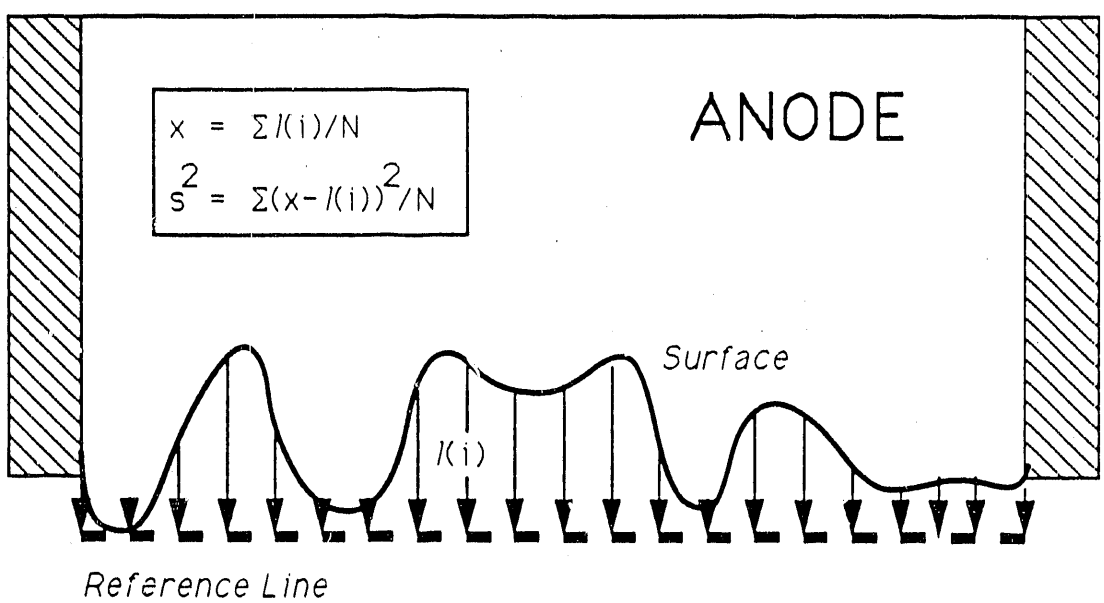

FIGURE 3.5. Illustration of Method for Quantifying Roughness of Cermet Anodes

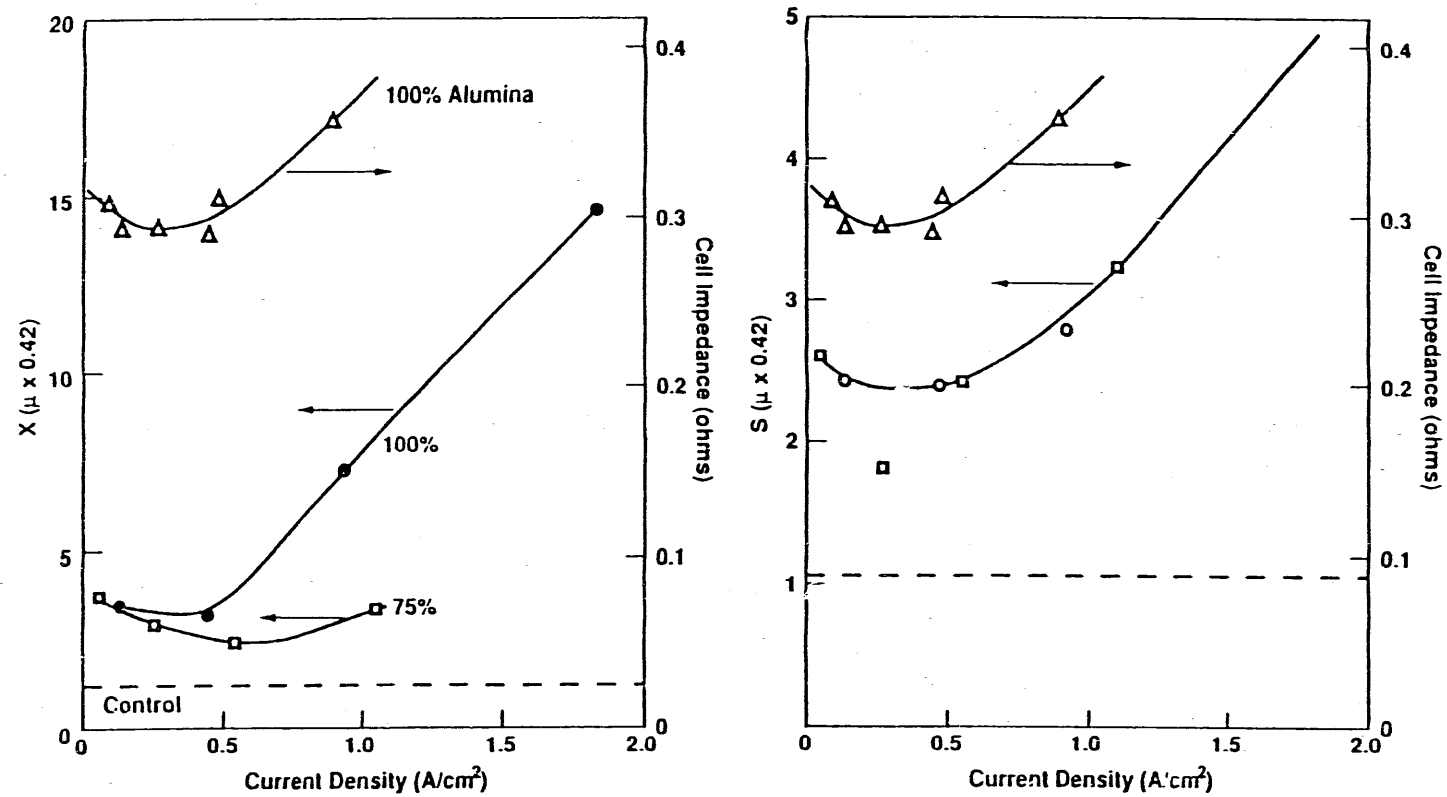

FIGURE 3.6. Relationships of Impedance and Roughness Factors x and s for Cermet Anodes. Data are for 100% (,) and 75% ( ) alumina and for an unpolarized control specimen(--).

Examination of Figure 3.3(a) shows that the surface roughening at lower current densities can be explained by extensive corrosion as deep as 100 μm into the anode. Figures 3.3(b) through 3.3(d) and Figures 3.4(b) through 3.4(d) show that the roughening at higher current densities was different. The subsurface of these anodes appears largely unaffected and reaction products were confined to the outer 10 to 20 μm of the material. Some possible reasons, based on compositional analysis, for the roughening associated with high current density, are discussed in Sections 3.4 and 3.5.

3.3.5 Surface Roughness and Electrochemical Impedance

The relationship between current density and surface roughness is similar to the variation between current density and cell impedance as determined previously (Windisch and Stice 1990). Impedance is highly dependent on cell geometry, including electrode area and topography. It is possible, therefore, that the observed relationship between impedance and current density is *caused* by changes in surface roughness, which in turn are determined by the anodic current density.

One possible explanation for the observed correlations is that only a portion of the total surface area is active, i.e., serves as a substrate on which the oxide ions are discharged. On a rough surface, the active regions would probably be the areas that protrude the most into the electrolyte. Recessed areas may be blocked by gas bubbles or, perhaps, solid, poorly conducting corrosion products. In any event, as a result of the roughening, a large portion of the surface area is rendered inactive, causing the "real" surface area to be less than that which is "apparent." The resulting impedance would be larger than expected.

The above explanation for the variation in cell impedance can also help explain certain issues that were puzzling in the context of the previously proposed alumina film-formation theory. First, the increase in impedance at lower current densities could not be explained because a protective film was believed not to form under these conditions. Also, in a number of previous studies at PNL it was observed that the anode impedance could be preserved when the anode was removed from the molten electrolyte and used at a later

date in another cell. This observation was explained by proposing that the film that formed on the anode could be preserved during the transfer, i.e., the film formed in the molten electrolyte under polarization conditions could exist intact on the electrode after its removal. This explanation is somewhat suspect since, as was discussed in Section 3.3.1, microscopic examination provided no evidence for such an intact layer. It is also improbable that any film could retain its chemical integrity considering the drastic physical and chemical changes accompanying the electrode transfer. It is more likely that the effects of surface roughness, a characteristic of the anode itself, would accompany the anode, surviving a transfer from one cell to another. Additional work is planned for FY 1991 to investigate further the source of the anode impedance.

3.3.6 Effect of Alumina Concentration

As shown by comparing Figures 3.3(a) through 3.3(d) with Figures 3.4(a) through 3.4(d), very similar morphological changes accompany the variation of current density at 75% and at 100% alumina. Between these alumina concentrations, at least, differences in corrosion properties do not appear to be significant in short-term laboratory-scale tests.

3.4 COMPOSITION OF THE REACTION ZONE

In this section, the results of optical microscopy, SEM (with EDS), and TEM (with electron diffraction) studies on the NiO-$NiFe_2O_4$-Cu cermet anodes will be discussed. As indicated in Section 3.3.1, no evidence for an intact, continuous film could be found on the anodes. All of the phases on the anode surface (which were not simply part of the frozen cryolitic bath) contained one or more of the cermet components (Ni, Fe and/or Cu). This argues against the formation of a film of alumina, which had previously been proposed by PNL.

The analyses reported here involved two parts of the reaction zone, which is diagrammed schematically in Figure 3.7. The first part, called the *anode reaction layer*, includes the cermet material right at the anode surface. Although still a solid, this material appears to have reacted with the molten electrolyte in some way. The first part of the reaction zone also includes

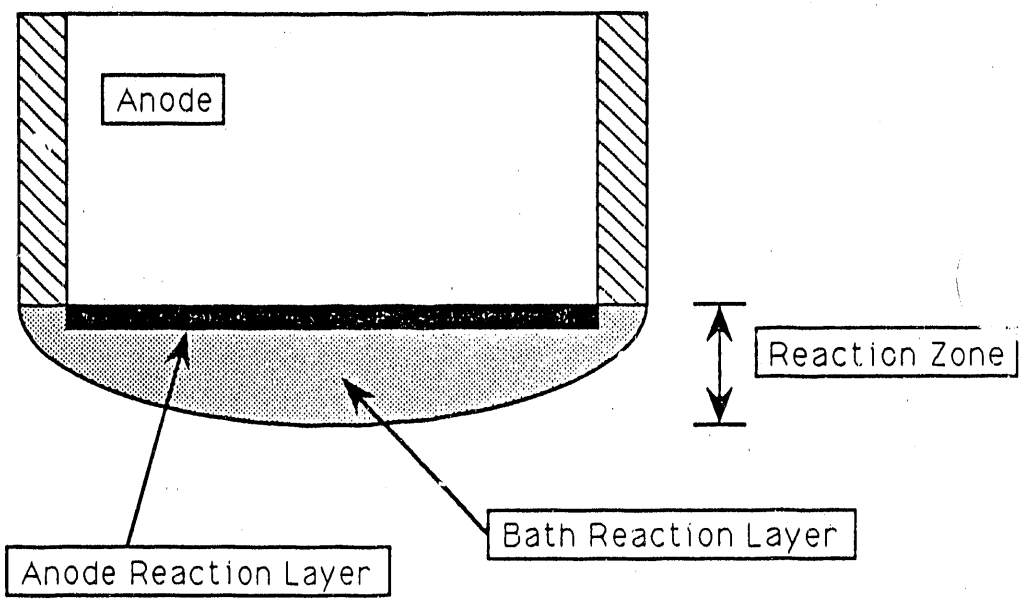

FIGURE 3.7. Schematic of Reaction Zone on Cermet Anodes

reaction products that may have precipitated from solution onto the anode surface. (The latter may not be distinguishable from the former.) The second part of the reaction zone, called the *bath reaction layer*, is the frozen electrolyte that adhered to the surface of the anode.

3.4.1 Anode Reaction Layer

Using SEM at magnifications of 1000X and higher, numerous phases can be identified that are clearly the result of interactions between the cermet material at the anode surface and the molten electrolyte. In all cases, these phases appear as discontinuous regions along the surface. Some phases appear as localized "extensions" of the oxide phases that make up the cermet, others as fibrous "swirls" extending from the anode surface, while others occur as isolated islands along the surface or within the melt near the anode surface. Only those phases that appear frequently along the surfaces or are considered especially important by the authors will be discussed here.

Only anodes tested at potentials higher than 2.2 V will be discussed in this section. As indicated in Section 3.3, at lower potentials, where minimal oxygen gas was produced, significant corrosion was observed. This corrosion

appeared different from the electrode wear observed at higher potentials and current densities. Since the data collected at higher current densities are more relevant to the anticipated normal operation of these anodes, the focus of this analysis will be on anodes polarized at potentials above 2.2 V. Also, the trend in roughness as a function of current density, illustrated in Figures 3.3 and 3.4 and summarized in Figure 3.6, points to a process that occurs with increasing intensity with increasing current density. Since anodes polarized to give higher current densities gave a greater *volume* of corrosion products within the 1-h test period, these tended to be the samples used for illustration in this report. However, compositional analysis of phases formed at all current densities above 2.2 V were similar and led to the same conclusions regarding the wear mechanism for the anode. As indicated in Section 3.3.6, varying the alumina concentration between 75% and 100% did not seem to have any significant effect on anode surface reactions. For these reasons, in the following analysis, samples of surfaces from a number of current densities and the two alumina concentrations are illustrated interchangeably. Similar effects were observed on all the anodes tested at 0.5 A/cm^2 and higher, but only micrographs of those that gave the best resolution of the various phases are presented here.

3.4.1.1 General Observations

The analyses reported here are for anodes EAT2SC and EAT3SB, whose test conditions are given in Table 3.2, and anode EAT11-1. EAT11-1 was a NIO-$NiFe_2O_4$-Cu cermet anode that was polarized at 2.5 V and 0.51VA/cm^2 under the same conditions detailed in the experimental section except that the molten electrolyte contained 1 wt% silica. As indicated previously, other short-term laboratory work indicated silica had no apparent effects on anode wear.

SEM micrographs at magnifications of 1000X and 3000X of part of the reaction zone for anodes EAT2SC, EAT3SB and EAT11-1 are shown in Figures 3:8,

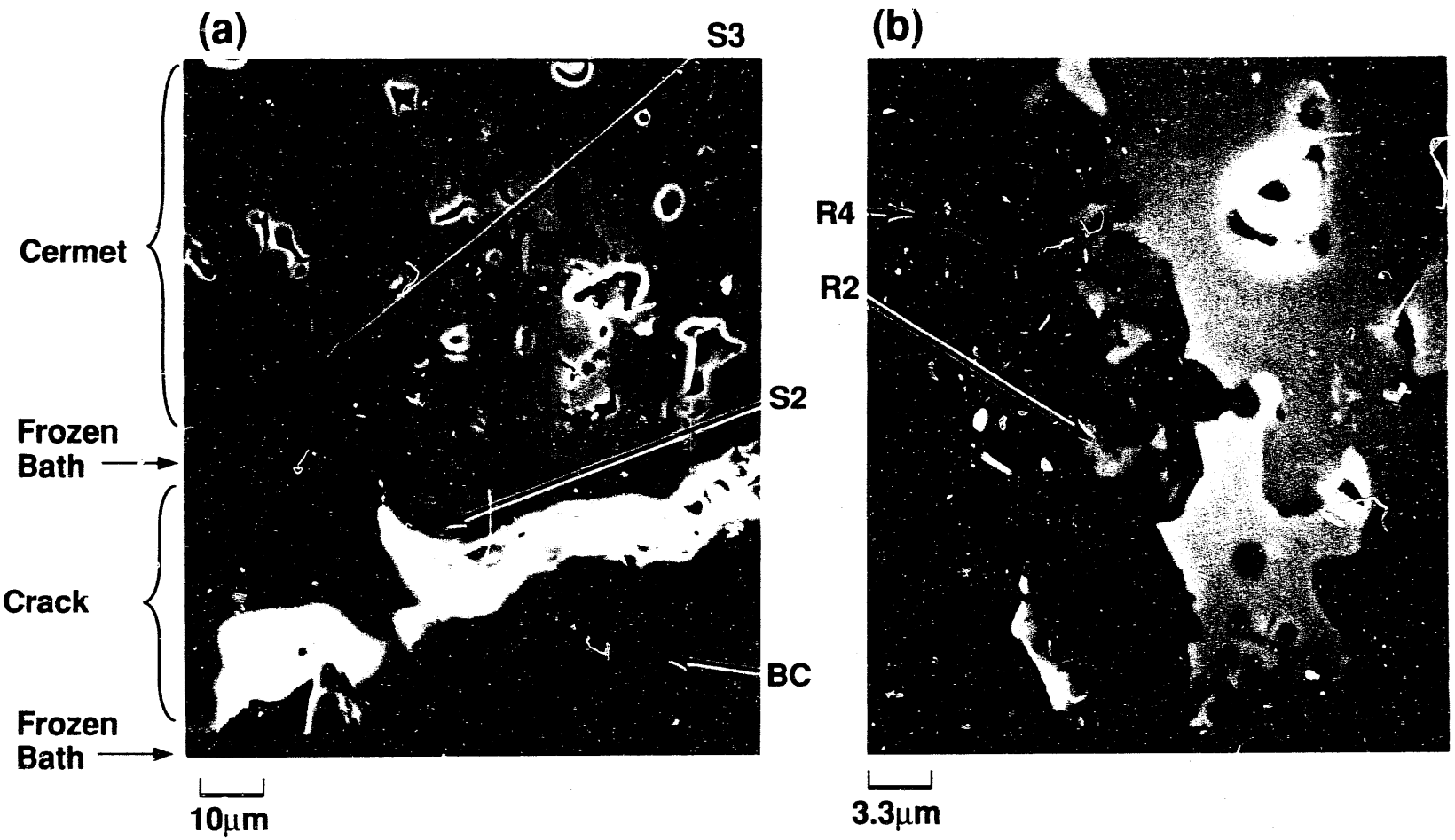

FIGURE 3.8. SEM Micrographs of Surface Region of Cermet Anode EAT2SC

3.9, and 3.10, respectively[a]. Under SEM analysis, it appears that polarization at potentials above 2.2 V had different effects on the three phases of the cermet anode. The NiO phase (which is light grey in the SEM micrographs) appears to be less affected by polarization than the $NiFe_2O_4$ phase (which appears dark grey in the SEM micrographs). As shown most clearly in Figures 3.8 and 3.10, the NiO phase extends further into the electrolyte than the $NiFe_2O_4$ phase, which is more "recessed." Some of the spinel phase has darkened near the surface as shown in Figure 3.9(b). This phase is labeled R1 and is referred to as reacted spinel. Swirls of fibrous-like reaction product also appear to be associated, at some locations, with the spinel. The swirls, labeled R2, can be seen clearly in Figure 3.9(b) and especially in Figure 3.8(b). In addition to these principal reaction phases, other less frequently occurring phases also formed [including R3 and R4 in Figures 3.9(a) and 3.8(b), respectively].

The Cu metal phase (which appears white or very light grey in the SEM micrographs) is almost nonexistent along the anode surface, indicating it has largely reacted in this region. Figure 3.10(b) appears to show part of the Cu phase in the process of reacting. The cavity contains reacted Cu (R5) and molten cryolite which has penetrated the anode (R6).

3.4.1.2 Reaction Products Involving the Oxide Phases

The compositions of the reacted spinel (R1) region, the fiber-like swirls (R2), and the other isolated reaction products (R3 and R4) had the compositions given in Table 3.3 as determined by EDS analysis. All of the phases appeared to be associated with or formed from the oxide phases of the original cermet material. The compositions of the bulk spinel ($NiFe_2O_4$) and the bulk cryolite (BC) are also given in Table 3.3 for comparison.

As shown in Table 3.3, two important similarities in the reaction products R1, R2, R3, and R4 are apparent. First, the concentration of Al in all

---

(a) As labeled in the SEM micrographs, the frozen bath usually cracked near the surface of the anode during cool-down. Some residual bath often remains on the anode surface. This bath was analyzed as reported later in the text.

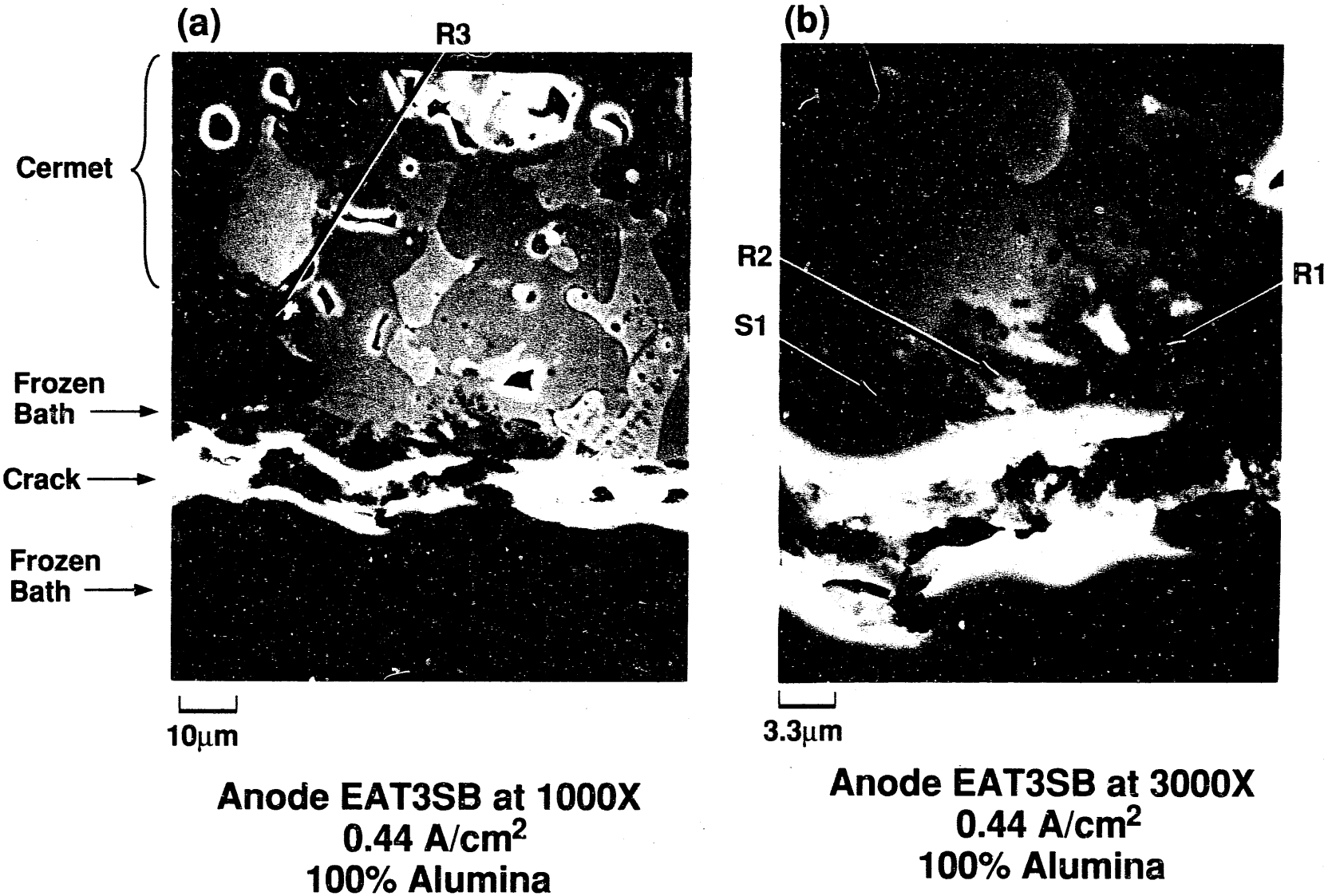

FIGURE 3.9. SEM Micrographs of Surface Region of Cermet Anode EAT3SB

39011044.6

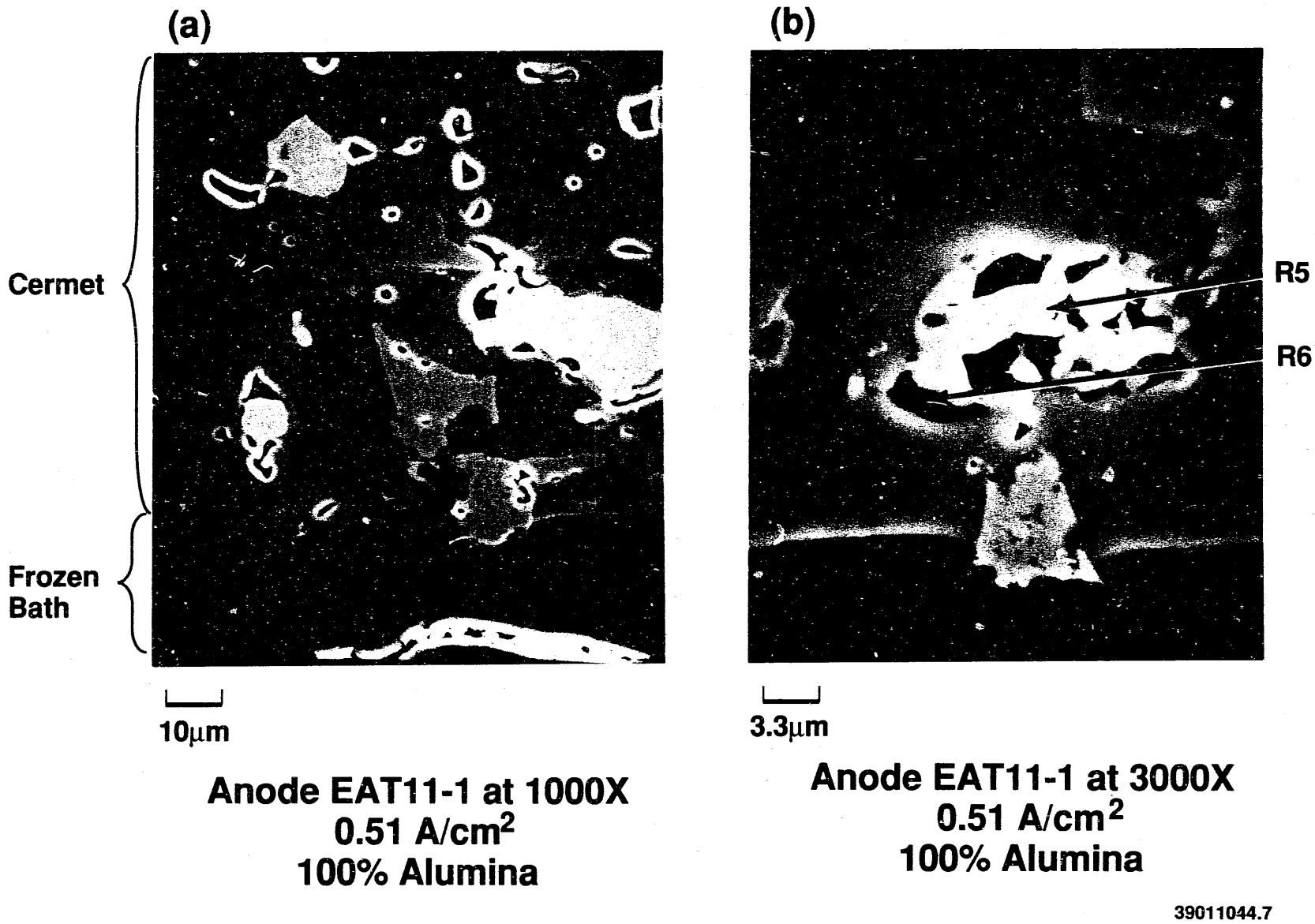

FIGURE 3.10. SEM Micrographs of Surface Region of Cermet Anode EAT11-1

TABLE 3.3. Elemental Composition of Reaction Products Involving Oxide Phases (wt%)

Anode	Phase	Na	Al	Si	Ca	Fe	Ni	Cu	Na/Al	Fe/Ni
EAT3SB	R1	5.6	31	0.4	1.4	8.3	10	3.9	0.2	0.8
EAT2SC	R2	12	35	0.7	0.7	15	20	0.9	0.3	0.7
EAT3SB	R3	0	37	0	0	8.4	16	11	0	0.5
EAT2SC	R4	28	44	0.7	2	6.9	11	4.5	0.6	0.6
EAT3SB	$NiFe_2O_4$	0	0	0.6	0	47	18	0.9	-	2.6
EAT2SC	BC	51	25	0.3	4.2	0.1	0.1	0.1	2.0	1.0

of these products is significantly higher than Na, unlike the bulk cryolite in which the concentration of the Na is higher than Al. This is shown by comparing the Na/Al ratios. For the reaction products, this ratio is 0.6 or smaller (zero in the case of R3), whereas for the bulk cryolite, the ratio is 2.0. Second, the concentration of Ni in all of the products is higher than Fe, unlike the bulk spinel in which Fe is higher than Ni. This is shown by comparing the Fe/Ni ratios. The ratio is less than one for the reaction products and 2.6 for the bulk spinel. For the stoichiometric $NiFe_2O_4$, the ratio is 1.9.

The reaction products clearly contain excess Al and excess Ni relative to either the bath composition or the spinel. One explanation for this is that they are all composed, at least partly, of a Ni-containing aluminate compound. Considering the composition of R3, which contains no significant amounts of Na, the Fe/Ni ratio is 0.5. On a *molar* basis, this corresponds to about 0.5 as well, suggesting an aluminate with the stoichiometry $Ni_2FeAl_xO_{(7+3x)/2}$. Interestingly, Alcoa (Baker 1983) proposed an aluminate $Ni_{1.33}Fe_{0.8}Al_{0.87}O_4$ (whose stoichiometry is close to the above formula) as an alternative to the spinel in the fabrication of cermet anodes because of its low solubility. The solubility of the aluminate is lower than that of NiO, Fe_2O_3, and even $NiFe_2O_4$.

The product R3 also contains Cu and Al in amounts that exceed those called for in the nickel-iron aluminate formula above. The Fe/Cu and Fe/Al mole ratios are 0.9 and 0.1 from the data in Table 3.3. The Cu might be

explained by the presence of copper aluminates such as $CuAlO_2$ and $CuAl_2O_4$. Both have been found on anodes in other laboratory tests at PNL and on the prototype anode (Windisch and Stice 1990; Strachan et al. 1990). A combined Ni-Fe-Cu aluminate might also be developed from the appropriate formulas. The very large excess of Al, however, suggests an even more complicated structure. More likely, R3 is an Al-rich solid solution containing Ni, Fe, and Cu, with Ni and Fe in relative proportions that are similar to the very stable nickel-iron aluminate. Unfortunately, attempts to identify R3 and the other reaction phases using different analytical techniques were unsuccessful. X-ray diffraction was not sensitive enough to identify the small quantities of this reaction product. The diffraction data were dominated by the bulk cermet oxides and the major frozen bath components. TEM and electron diffraction applied to the anode reaction layer in thin sections of the polarized anodes were also unsuccessful because a thin enough sample of the electrode material could not be made. When TEM was applied to the bath reaction layer, the electron beam was found to interact strongly with the fluoride-containing components.

As shown in Table 3.3, the other reaction products R1, R2, and R4 also contained significant amounts of Na, which suggests some cryolite was also being detected by the probe for these samples. This is reasonable since these products extended more into the frozen electrolyte than R3 as shown in Figures 3.8(b) and 3.9(b). The presence of cryolite makes precise stoichiometric determination from the EDS data difficult since the Al is associated not only with possible aluminate compounds but with the cryolitic components as well. In all cases, however, the Fe/Ni ratios are similar and not too different from the 0.5 used in the calculations on R3. This suggests that all of these phases exhibit some similarity to the stable nickel-iron aluminate composition discussed above. The electron microprobe line scans for sample EAT2SC shown in Figure 3.11 corroborate this finding. The linescan for Al shows a peak near the anode interface whose position correlates with the onset of signals from Fe and Ni. This indicates that significant amounts of Al are present at the anode surface.

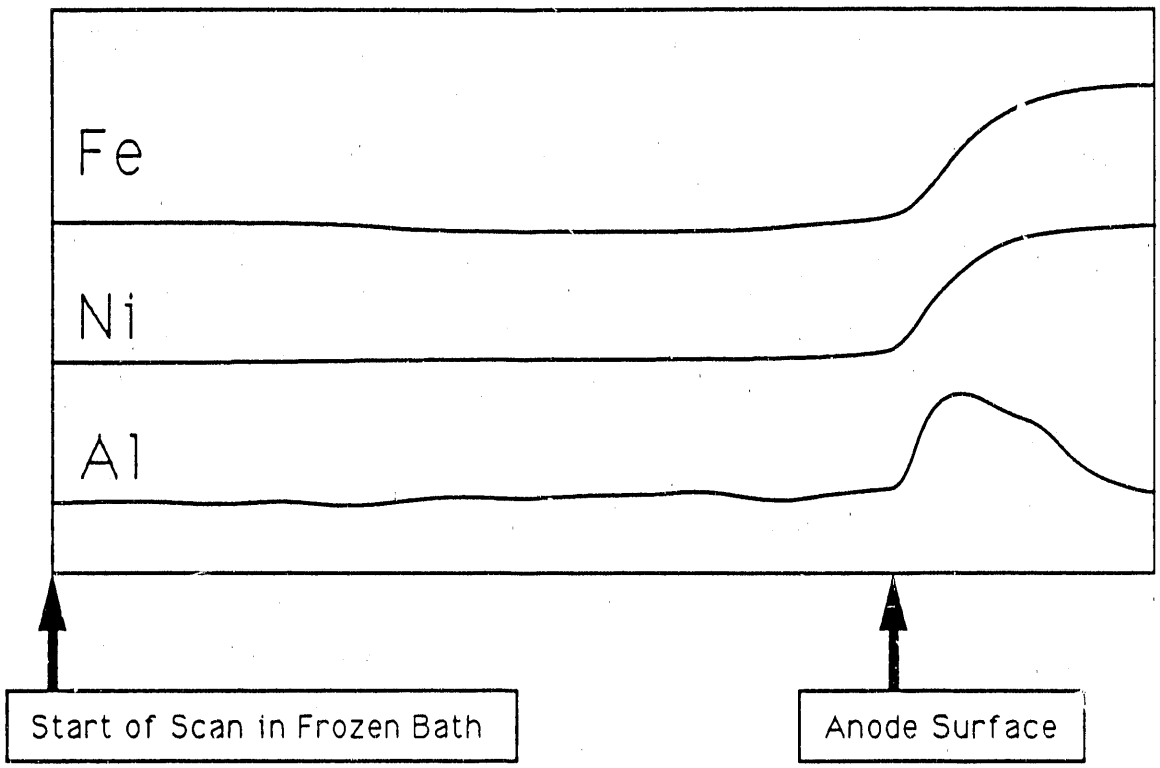

FIGURE 3.11. Electron Microprobe Linescans of Cermet Anode EAT2SC

It is also interesting that the relative amounts of Cu in R1, R2, and R4 are less than in R3. For example, in R1 the Cu/Fe ratio is 0.5 compared to 1.3 in R3. This suggests that R3 may have formed nearer the Cu metal phase than the other reaction products. Referring to Figure 3.9(a), R3 occurs adjacent to a cavity. Based on the above analysis, it is reasonable that the cavity was created by the voiding of a Cu particle. This possibility is supported by the results of analysis of the Cu metal phase as discussed in Section 3.4.1.3.

The results reported here indicate that the primary solid reaction products formed near the cermet anode surface during polarization contain more Ni than Fe. Even the reaction product R1, which appears as an extension of the spinel phase, exhibits excess Ni. This means that more Fe than Ni in the spinel must be lost to solution during electrolysis. Since the spinel phase appears to show a greater amount of dissolution than the NiO in these

short-term tests, as discussed in Section 3.4.1.1, the mechanism for Fe dissolution would appear to be an important part of the overall wear process.

3.4.1.3 Reacted Cu Metal Phase

The absence of significant amounts of Cu metal at the anode surface suggests the Cu phase is corroded into the electrolyte from the surface regions during electrolysis. Figure 3.10(b), which shows a portion of the Cu phase undergoing dissolution, provides some additional insight into the processes. The composition of the reacted Cu (R5) is compared with that of bulk metallic phase (Cu), and the composition of the molten cryolite near the Cu (R6) is compared with that of the bulk (BC).

As shown in Table 3.4, the reacted Cu phase (R5) is severely depleted in Ni compared to the bulk (Cu), and the cryolite near this phase (R6) contains significant amounts of Ni, Fe, and Cu. Clearly, the alloy is dissolving. Given the relative amount of the three metals in the metallic phase, it appears that Ni has the greatest tendency to "dealloy itself." The high amounts of Fe in the cryolite cannot be explained by dealloying since significant amounts of Fe remain in the reacted Cu phase. More likely, the Fe came from the spinel phase, which borders the Cu metal phase.

The anode shown in Figure 3.9(a) contains the reaction product R3. The hole in the surface was probably formed as a result of Cu metal phase dissolution. As reported in Section 3.4.1.2, the analysis of R3 suggests the presence of a copper aluminate or a Cu-containing solid solution that apparently accompanies the dissolution of the Cu metal. No evidence was found that copper aluminate compounds passivate the metal phase.

TABLE 3.4. Elemental Composition of Reaction Products Involving the Cu Metal Phase (wt%)

Anode	Phase	Na	Al	Si	Ca	Fe	Ni	Cu	Na/Al	Fe/Ni
EAT11-1	R5	0	0	0.6	0.1	3.7	1.0	71	-	3.7
EAT3SB	Cu	0	0	0	0	3.2	10	83	-	0.3
EAT11-1	R6	50	13	0.5	0.6	15	5.7	8.8	3.8	2.6
EAT11-1	BC	51	25	0.3	4.2	0.1	0.1	0.1	2.0	1.0

3.4.2 Bath Reaction Layer

Four samples of cryolite bath near the anode surface were analyzed in this work: (S1) adjacent to the spinel phase shown in Figure 3.9(b), (S2) adjacent to the NiO phase shown in Figure 3.8(a), (S3) adjacent to the spinel phase in the interior of a cavity, and (BC) further removed from the anode surface [Figure 3.8(a)]. BC is referred to as a bulk sample. It was only 30 μm from the surface of the anode, but on the microscopic scale, it was considered far enough away to serve as a reference for comparing compositions. In contrast, S1 through S3 were sampled about 3 μm away from the surface. The results of these analyses are given in Table 3.5 along with data for the bulk spinel for comparison.

The Na/Al ratios for S2 and S3 are essentially the same as the bulk composition, while S1 may exhibit a slightly larger Na/Al ratio. The Fe/Ni ratio for S1 is very close to the spinel composition. This would suggest the spinel is dissolving nearly stoichiometrically. Formation of a nickel-iron aluminate (as discussed in Section 3.4.1.2) should keep more Ni than Fe out of solution and would predict a larger Fe/Ni ratio. The smaller Fe/Ni ratio may have been due to one or more of the following three factors: (a) the presence of a nearby NiO phase may have augmented the Ni content of this region; (b) some Fe may have been scrubbed from solution by gaseous oxygen and/or volatilized as iron fluoride compounds; and (c) the dissolution of the Fe may have slowed down after some initial period. Possibility (b) was proposed to explain the concentrations of Fe dissolved in Al during recent PNL laboratory-scale studies. S2 and S3 also showed higher Ni contents, which could be due

TABLE 3.5. Elemental Composition of Bath Reaction Layer (wt%)

Anode	Phase	Na	Al	Si	Ca	Fe	Ni	Cu	Na/Al	Fe/Ni
EAT3SB	S1	53	20	0.4	2.7	0.4	0.2	0	2.6	2.0
EAT2SC	S2	52	24	0	2.8	0.3	0.5	0.1	2.2	0.7
EAT2SC	S3	49	25	0.3	2.8	0.3	0.3	0	2.0	1.0
EAT2SC	BC	51	25	0.3	4.2	0.1	0.1	0.1	2.0	1.0
EAT2SC	$NiFe_2O_4$	0	0	0.6	0	43	20	1.1	-	2.2

to the presence of a nearby NiO phase according to (a). NiO is clearly present in the case of S2, and the large cavity bordering S3 [Figure 3.9(a)] may have contained some of the NiO phase at one time. Kinetic factors such as (c) may also be important as discussed in Section 3.5.

3.5 PROPOSED REACTION SCHEME FOR ANODE WEAR

The principal results of this work concerning reactions at the cermet anode surface were the following:

- The cermet anodes roughened on polarization.
- The roughening appears to have been caused by three factors: loss of Cu metal near the surface, protrusion of the NiO phase into the electrolyte, and erosion of the spinel phase.
- The Cu metal phase corroded/dissolved near the surface region. It appeared that the Ni component of the alloy oxidized first, followed by Cu metal itself.
- The eroded spinel showed a non-continuous reaction region that was Fe-depleted and Al-rich. Other reaction products near the anode surface showed this same pattern in composition.
- No reaction region similar to the spinel was observed on the NiO phase near the surface. In these short-term tests it appeared that the NiO phase was more resistant to reaction/dissolution than the spinel phase.
- The electrolyte near the anode did not contain an excess amount of Fe as would be expected if Fe were dissolving selectively.

The above results will be discussed in the following two sections: Section 3.5.1 covers the results on the Cu metal phase, and Section 3.5.2 covers the results on the oxide phases. In these sections, some reactions are proposed that are consistent with the results. Since definitive analytical data (i.e., identifying phases and chemical moieties *under operating conditions*) were not available in this work, explanations other than those presented in this report may also be possible. The following proposals were considered most feasible by the authors in light of other PNL research and previous work at Alcoa Laboratories (Weyand et al. 1986).

3.5.1 Reactions Involving the Cu Metal Phase

This work corroborates the findings in other laboratory cell tests and the prototype anode test (Strachan et al. 1990). The results indicate that the Cu metal phase is depleted near the surface of the anode during electrolysis. Moreover, part of the oxidation/dissolution process appears to be the selective oxidation of the Ni component of the metallic phase. The present work showed one of the first illustrations of part of the Cu metal phase *in the process of dissolving* [Figure 3.10(b)].

3.5.2 Reactions Involving Oxide Phases

The results of this work concerning the oxide phases appear to indicate that Al exchanges for Fe in the anode reaction layer. A number of mechanisms for this exchange are possible. For example, the Al^{3+} ion may exchange for Fe^{3+} in the spinel lattice, or the spinel may decompose to give another crystalline oxide or a solid solution containing predominantly Al and Ni oxides and fluorides. With the current data we are unable to distinguish definitively between these and other possible mechanisms. However, previous work by Alcoa laboratories provides some clues to a likely mechanism.

As indicated at the beginning of this section, it appeared that the NiO phase did not dissolve as quickly as the spinel, at least initially. The preferential dissolution of the spinel was surprising in light of work by Alcoa (Weyand et al. 1986). Alcoa showed that $NiFe_2O_4$ exhibited much lower solubility than NiO in a series of solubility studies. (Fe_2O_3 exhibited a higher solubility.) Moreover, their cermet inert anodes, which were subjected to electrolysis for times longer than those in this study, showed an outer layer of $NiFe_2O_4$ without any significant amount of NiO, suggesting that the spinel was less soluble than the NiO. In the prototype anode test as well, the outer surface of the anode was depleted in Ni (Strachan et al. 1990). But in the tests reported here the NiO did not appear to react with the cryolite as it did with the spinel. No "reaction regions" characterized by high Al were observed on the NiO.

The spinel may have been more reactive with the molten bath because of the presence of excess Fe, presumably in the Fe^{2+} state as indicated earlier. As discussed by Alcoa (Weyand et al. 1986), FeO oxidizes according the following reaction at 2.36 V:

$$FeO + AlF_3 \text{ ---> } FeF_3 + 1/2\ O_2 + Al$$

where the activity of AlF_3 is 1.5×10^{-3} at 1250 K. The corresponding anodic *half-reaction* is

$$FeO + AlF_3 \text{ ---> } FeF_3 + 1/2\ O_2 + Al^{3+} + 3e$$

A reaction like this may occur locally at Fe^{2+} sites within the spinel oxide matrix at potentials above 2.36 V resulting in the production of iron fluoride and aluminum ions. The fluoride may dissolve away or volatilize while the Al^{3+} remains behind as part of the oxide or a component of a new solid solution depleted in Fe ions.

The above reactions with Fe^{2+} in the spinel phase may also occur with Fe^{2+} in the NiO phase although, apparently, to a lesser extent since the NiO does not develop the same kind of reaction layer, at least in the short term. Rather, the results of these short-time exposures showed significant amount of the NiO phase near the surface, mainly as protrusions of the roughened cermet surface. When sufficient amounts of the spinel erode during the early dissolution step, the NiO phases may "fall out," contributing to the rough morphology observed in this work.

Over longer times, the morphology will be determined by the chemical and physical properties of the reaction products. The spinel reaction layer, typified by phase R1 in Figure 3.9(b) may "spread out" over the entire spinel surface as NiO "falls out" and more and more of the spinel is exposed to the electrolyte. If the spinel phase is the predominant component of the anode near the surface after extended periods of polarization (as indicated by the work by Alcoa and PNL), it would appear that the reaction layer on the spinel is *protective*. Continued fall-out of the NiO phase coupled with the slow-down

of the spinel dissolution due to the protective reaction phase may result in the microstructure observed in other longer-term studies: a surface morphology with a composition characterized mostly by spinel. The absence of excess amounts of Fe in the electrolyte near the anode surface also supports this mechanism. Once the protective phase develops, less Fe dissolves and hence less is measured in the electrolyte near the protected regions.

The precise identity of the reaction layer is still uncertain. This work indicates that it is not a film (e.g., of alumina) formed from solution components only, as was previously proposed. The reaction layer contains electrode components in addition to electrolyte components. The layer is rich in Al and appears to form mainly from the spinel phase but is depleted in Fe relative to the spinel. The phase may be crystalline or amorphous. It may be a solid solution that somehow acts as a barrier for the diffusion of aggressive electrolyte ions. Whatever the explanation may be, the data, when compared with previous results from this laboratory and others, seem to indicate the reaction phase is protective. Once formed, it may slow down the dissolution of the oxide phase and, perhaps more importantly, control the access of the electrolyte to the oxidation-sensitive Cu metal phase.

The contribution of the reaction layer to measured electrochemical impedances is also uncertain at this time, since it cannot be distinguished from other factors (such as roughness) and processes (such as oxygen evolution) that occur simultaneously. Experiments are currently under way to identify the various sources of the anode impedance.

A schematic of the proposed reaction scenario is shown (in a somewhat exaggerated format) in Figure 3.12. Cu reacts/dissolves in the surface region of the cermet anode under polarization. The NiO phase dissolves slowly but "leaves" more suddenly in the short term as a result of "fall out." The spinel phase dissolves quickly in the short term until a reaction layer forms that slows down the dissolution process.

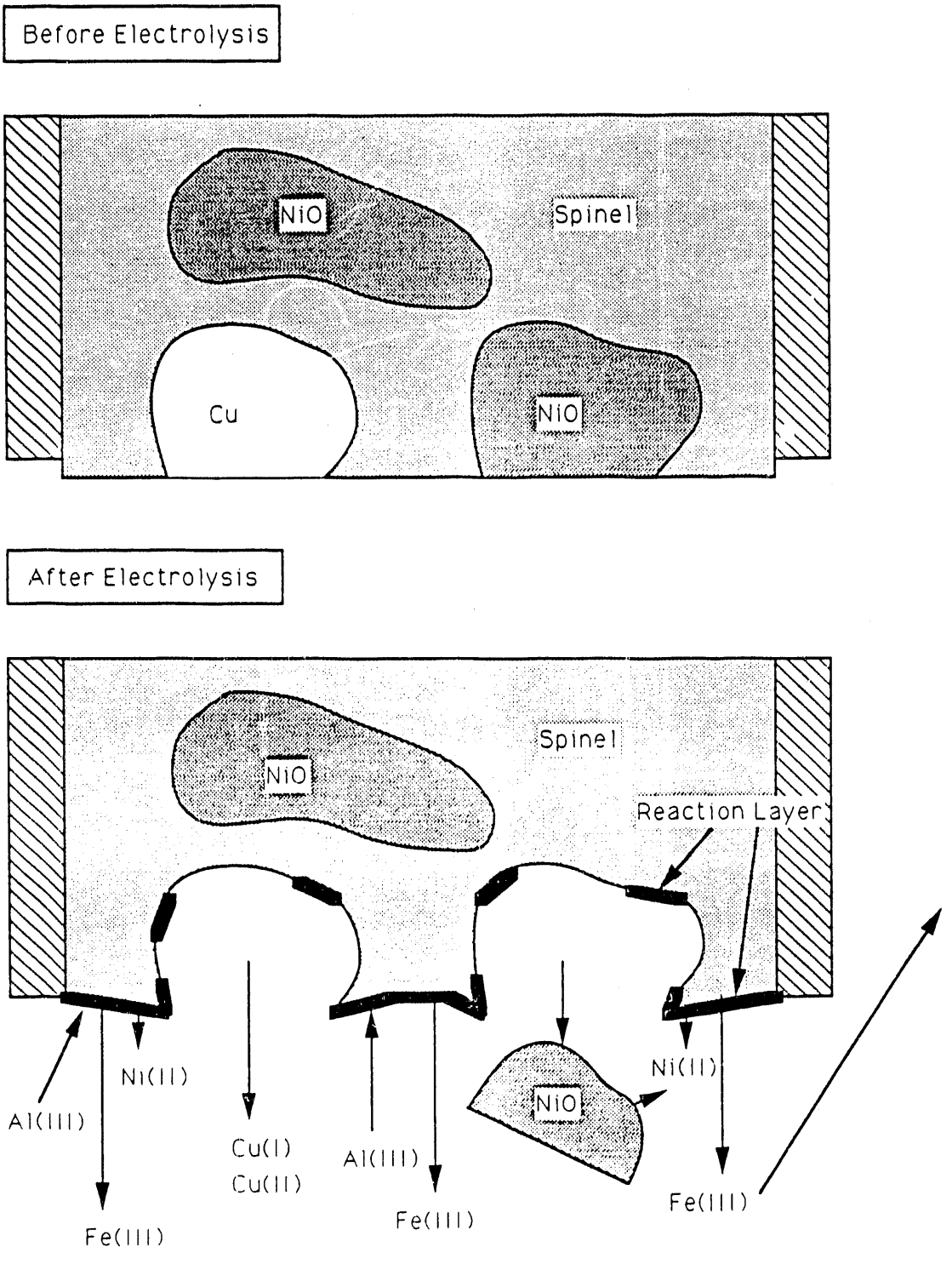

FIGURE 3.12. Schematic of Proposed Reactions/Processes at the Cermet Anode Surface During Electrolysis

3.6 RECOMMENDATIONS BASED ON PROPOSED REACTIONS

If the spinel reaction layer is protective, as appears to be the case, those factors that favor its formation would be desirable. Given the elemental composition of the layer, these factors include the following:

- higher amounts of Al in the bath (especially in the form of alumina since the oxyfluorides migrate to the anode during electrolysis)
- polarization above the potential required for Fe^{2+}-component decomposition (approximately 2.39 V)
- optimization of a microstructure that would minimize the effects of NiO fall-out and favor the transition to a uniform reaction-layer-coated spinel surface.

Interestingly, the first two factors were already shown to be important. Alcoa (Weyand et al. 1986) demonstrated the need to maintain alumina concentrations near saturation to minimize the solubility of the cermet. The second factor was demonstrated by PNL, as discussed in Section 3.3, in tests at anode potentials below 2.2 V. The effect of microstructure has also been anticipated, and research in this area in currently under way at PNL.

4.0 CONCLUSIONS

Results of post-test microscopic and elemental analysis of the reaction zone on polarized cermet inert anodes, over a range of current densities and alumina concentrations, suggest that an alumina film does not form to protect the anode from dissolution. Rather, significant morphological and compositional changes occur at or near the anode surface. These changes and the chemical reactions that cause them involve the cermet material itself and appear to be responsible for properties that were previously assigned to an alumina film. The changes include an increase in surface roughness with current density and the formation of a reaction layer predominantly on the spinel phase. The roughness appears to be caused by different reactivities of the phases in the cermet material and may contribute to the previously determined variations in electrochemical impedance. The reaction layer is rich in Al and depleted in Fe relative to the spinel, but its crystallographic form has not yet been determined. It may, in fact, be a solid solution containing both anode and bath components. Comparison with the results of other studies suggests the reaction layer may be protective.

5.0 REFERENCES

Baker, F. W. 1983. Inert Anodes for Aluminum Smelting: Final Technical Report for the Period 1981 October 01 - 1982 September 30. DOE-CS-40158, Alcoa Laboratories, Alcoa Center, PA.

Burgman, J. W., J. A. Leistra, and P. J. Sides. 1986. "Aluminum/Cryolite Reference Electrodes for Use in Cryolite-Based Melts." J. Electrochem. Soc. 133(3):496-500.

Strachan, D. M., O. H. Koski, S. C. Marschman, C. H. Schilling, and C. F. Windisch Jr. 1988. Fiscal Year 1987 Annual Report for the Inert Electrodes Program. PNL-6746, Pacific Northwest Laboratory, Richland, WA.

Strachan, D. M, C. F. Windisch Jr., O. H. Koski, L. G. Morgan, R. D. Peterson, N. E. Richards, and A. T. Tabereaux. 1990. Results from Electrolysis Test of a Prototype Inert Anode. PNL-7345, Pacific Northwest Laboratory, Richland, WA.

Weyand, J. D., D. H. DeYoung, S. P. Ray, G. P. Tarcy, and F. W. Baker. 1986. Inert Anodes for Aluminum Smelting: Final Technical Report for the Period 1980 September 29 - 1985 September 30. DOE-CONS-40158-20, Alcoa Laboratories, Alcoa Center, PA.

Windisch C. F., Jr., and N. D. Stice. 1990. Characterization of the Reaction Layer or Film on PNL Inert Anodes: Progress Report for April-December 1989. PNL-7326, Pacific Northwest Laboratory, Richland, WA.

END

DATE FILMED

03/01/91